Impact of citric acid on the impregnation of CoMoP/γ-Al 2 O 3 catalysts: time and spatially resolved MRI and Raman Imaging study

L. Catita, A.-A. Quoineaud, M. Moreaud, D. Espinat, C. Pichon, O. Delpoux

Impact of citric acid on the impregnation of CoMoP/γ-Al_2O_3 catalysts: time and spatially resolved MRI and Raman Imaging study

L. Catita[a], A.-A. Quoineaud[a], M. Moreaud[a,b]; D. Espinat[a], C. Pichon[a], O. Delpoux[a,*]

[a]*IFP Energies Nouvelles, Rond-point de l'échangeur de Solaize BP3, 69360 Solaize (France)*

[b]*MINES ParisTech, PSL-Research University, CMM, 35 Rue Saint Honoré, 77305 Fontainebleau*

**Corresponding author: olivier.delpoux@ifpen.fr (Tel. +33(0) 4 37 70 23 18)*

Abstract

An *in-situ* characterization methodology based on the Magnetic Resonance Imaging (MRI) and Raman Imaging is applied to investigate the effect of citric acid in the impregnation step of molybdenum catalysts promoted with cobalt in the presence of phosphorus and support on γ-alumina. MRI provides temporal and spatial information of the transport of species of the impregnation solutions within the porosity with a spatial resolution of 39×39µm. Raman Imaging gives information about the chemical nature of the species deposited on the support with a spatial resolution of 16.2×16.2µm. The effect of citric acid strongly depends on the ratio between the additive and molybdenum used in the impregnation solution. For a ratio of 0.2, at the end of impregnation, molybdenum ions are in an egg-yolk distribution either in polymeric or monomeric form. For a ratio of 0.7, cobalt ions can be in the form of aqua complexes in an egg-yolk distribution or in the form of $H_2PMo_{11}CoO_{40}^{5-}$ heteropolyanion, which can improve the proximity between molybdenum and cobalt ions. This work gives new insights concerning the role of citric acid on the metal distribution profiles obtained at the end of impregnation, which can be used to control the final active phase distribution.

Keywords:

Hydrotreatment, Impregnation, Citric Acid, MRI, Raman Imaging

Abbreviations

CA, Citric Acid; EPMA, Electron Probe Microanalysis; HDT, Hydrotreatment; MRI, Magnetic Resonance Imaging; NMR, Nuclear Magnetic Resonance; TR, Repetition time; TE, Echo time

1. Introduction

Nowadays, there is a growing need of hydrotreatment (HDT) processes due to two main reasons: emergent need of reduction of sulfur content not only in gasoline, but also in diesel and increasing use of heavier crudes with high amount of sulfur [1].

A heterogeneous HDT catalyst consists of a metallic sulfide phase composed of a metal from group VI (generally molybdenum, Mo or tungsten, W) promoted or not by a metal from group VIII (usually nickel, Ni or cobalt, Co). Typically, the concentration by weight of these metals is 1-4% for Co and Ni, 10-25% for Mo and 12-25% for W [2]. This phase is dispersed on the surface of an inorganic oxide support, commonly γ-alumina, δ-alumina, silica or even silica-alumina [2].

The preparation of HDT catalysts consists in a series of unitary steps. The deposition of the active components is commonly obtained by incipient wetness impregnation, which consists in filling the porous volume of the support with a solution containing the active metal precursor and sometimes other additives. After that, an ageing step takes place, followed by thermal treatments (drying and eventually calcination). The active phase is obtained by a sulfidation reaction, during which most of the oxide phases are transformed into a transition metal sulfide (TMS) - Co(Ni)Mo(W)S.

To improve the performance of HDT catalysts, it is essential to obtain an optimal dispersion by distributing uniformly the precursors of the active phase and to limit their interaction with the surface of the support [3]. These phenomena can be controlled during the impregnation step, since at this stage most of the initial dispersion and the chemical structure of the metal species are determined.

In a recent work, in order to identify the descriptors that most influence this preparation step, we applied for the first time Magnetic Resonance Imaging (MRI) to monitor *in-situ* the impregnation of a real HDT catalyst [4]. This means that an aqueous solution composed simultaneously of molybdenum, cobalt and eventually phosphorus was used as impregnation solution. A significant improved spatial resolution of 39 μm × 39 μm compared to the literature was also achieved. Additionally, Raman Imaging was used to obtain spatial information concerning the chemical nature of molybdenum species deposited in the support at equilibrium. This innovative Magnetic Resonance Imaging-Raman Imaging methodology enables, for instance, to put in evidence a weakening of the interactions between alumina and molybdenum as a result of a preferential adsorption of phosphorus onto the support. This phenomenon, which is independent of the presence or not of the promotor results in an increase in the transport rate of molybdenum complexes. Besides, in the presence of phosphorus, preferential interactions between cobalt and alumina are observed rather than with molybdenum species.

Nevertheless, since several years, numerous studies reported about the role of organic additives as complexing agents, in particularly citric acid. When introduced with the metallic precursors in the impregnation solution, citric acid can increase the active phase active dispersion, improve the solubility of the species and contribute to the formation of heteropolyanions [5–12].

In the present work, we apply the same Magnetic Resonance Imaging- Raman Imaging methodology in order to give new insights into the impact of citric acid on impregnation step CoMoP/γ-Al_2O_3 catalysts. In particular, the

influence of citric acid concentration in the impregnation solution is investigated. The combination of MRI and Raman Imaging techniques allows following the transport of the impregnation solution in terms of time, position in the catalyst pellet and chemical nature.

2. Experimental Methodology

2.1. Impregnation solution

Molybdenum impregnation solutions with a concentration of 0.8M [Mo], which corresponds to 6.9 wt% Mo (1.6 Mo atoms/nm^2) in the final catalyst, were prepared from ammonium heptamolybdate ($(NH_4)_6Mo_7O_{24}$) of 100 % purity (VWR BDH Prolabo). Mo precursor was dissolved in a certain quantity of deionized water and oxygen peroxide H_2O_2 of 30% of purity. Phosphorus was added in the form of phosphoric acid (H_3PO_4) of 85.0% purity in a P:Mo ratio equal to 0.4 (molar). Cobalt nitrate ($Co(NO_3)_2.6H_2O$) of 98.0% purity (Alfa Aesar, CAS number 10026-22-9) was added in a Co:Mo ratio equal to 0.3 (molar) to the impregnation solution when needed. Citric acid ($C_6H_8O_7$) of 99.5 wt.% purity (Sigma-Aldrich, CAS number 77-92-9) was introduced with the metallic precursors in impregnation solution (co-impregnation). Two different ratios CA:Mo were tested in order to investigate a possible complexation of Mo by citrate so as to form $Mo_4(Cit)_2O_{11}^{4-}$ complex. Therefore, CA:Mo ratio was varied from 0.2 (below stoichiometric ratio of CA to Mo in favour of the complex, namely 0.5) to 0.7 (above stoichiometric ratio of CA to Mo). Table 1 gathers the characteristics of impregnation solutions used in this study.

Table 1 – Chemical composition of impregnation solutions

Solution	[Mo] (M)	[P] (M)	[Co] (M)	[CA] (M)	pH
CoMoP-CA(0.2)	0.80	0.32	0.24	0.16	< 1
CoMoP-CA(0.7)	0.80	0.32	0.24	0.56	< 1

2.2. Impregnation method

An industrial pre-shaped γ-Al_2O_3 in the form of trilobal extrudate, prepared by kneading-extrusion of boehmite powder, with 1.2-1.3 mm diameter and 3-6 mm of length was used as support. The textural properties of the support were obtained by mercury porosimetry and nitrogen adsorption-desorption methods. This support is characterized by a total porous volume of 0.6 cm^3/g and a specific surface S_{BET} of 250 m^2/g. The point of zero charge (PZC) is 8-8.5. The high specific surface area of the support allows the dispersion of the active phase, while its trilobal shape aims to prevent from diffusional limitations during the HDT process.

Impregnation was performed in diffusional conditions as described in an earlier study [4]. One alumina pellet (pre-saturated with water) was put in contact with the impregnation solution containing the active elements for 30s, being the excess solution removed by a wiping. The sample was then introduced in a 5 mm thick wall NMR tube having heavy wall thick of 1.4 mm in order to perform MRI characterization. The composition of the final solid was obtained through EPMA technique. Lower concentrations of each element (Mo, P and Co) than the ones expected by incipient wetness impregnation method were obtained, since in the present preparation method the support was first saturated with water and then the impregnation step was performed.

2.3. Description of the MRI-Streamline Raman methodology

2.3.1. Magnetic Resonance Imaging (MRI)

MRI experiments were performed in a Bruker Avance 400MHz (^{1}H) spectrometer, which produces a homogeneous and stable superconducting magnetic field $\overrightarrow{B_0}$ (9.4 T). This spectrometer is equipped with a 5mm imaging probe (Micro5) and xyz gradient amplifiers (750×750×750 G/cm), which allows the voxels of interest to be selected. Experiments were carried out at 17°C temperature.

2.3.1.1. Measurement of relaxation times T_1 and T_2

Contrast of ^{1}H MRI images is obtained using the relaxation times (T_1 and T_2) of the proton. Therefore, a RAREVTR (Rapid Acquisition with Relaxation Enhancement with variable repetition time TR) sequence, which is based on multiple-echo sequence was applied to measure simultaneously T_1 and T_2 [13–15]. Relaxation times obtained are summarized in Table 2.

Table 2 – Relaxation times of the proton obtained in the presence or not of contrast agents

System	Relaxation times (ms)	
	T_1	T_2
$H_2O/\gamma\text{-}Al_2O_3$	370	3.9
$Co/\gamma\text{-}Al_2O_3$	15	2
$Mo/\gamma\text{-}Al_2O_3$	665	4.2
$H_3PO_4/\ \gamma\text{-}Al_2O_3$	935	7
CA/γ-alumina	468	3.8

2.3.1.2. MRI sequence

^{1}H MRI images were obtained by applying a spin-echo sequence, which consists of a 90° pulse, a 180° pulse and then an echo. The time between 90° pulse and the echo is called echo time (TE). The sequence was repeated at time TR (repetition time). Relation between these parameters is given by Eq. 1.

$$M(t) = M_0\left(1 - e^{-TR/T_1}\right)e^{-TE/T_2} \qquad \textbf{Eq. 1}$$

Where, M(t) represents the magnetization, M_0 the magnetization at equilibrium, TR the repetition time, TE the echo time, T_1 the spin-lattice relaxation and T_2 the spin-spin relaxation.

During this sequence, three different gradients are applied: slice-selection gradient (G_s), a phase-encoding gradient ($G_ø$) and a frequency-encoding gradient (G_f).

Images are characterized by a field of view (FOV) of 2.5×2.5×8 mm and 64×64×8 acquisition points, resulting in a voxel size of 39 µm×39 µm×100 µm. The total scan time was 17min 4s (TR and TE were equal to 500 ms and 2.2 ms, respectively). Paravision 5.1 software was used for MRI images acquisition.

2.3.2. Raman spectroscopy analysis

Raman spectroscopy was performed with a Renishaw inVia Raman microscope in backscattering configuration using the excitation line of 532 nm provided by a NdYAG laser equipped with EasyConfocal Renishaw device. The diffuse light was dispersed with a 2400 lines/nm grating, which allows an optimal spectral resolution around 0.9 cm^{-1}.

Concerning the measurements of the impregnation solutions, Raman spectra were acquired from 60 to 1300 cm^{-1} and the laser beam was focused with a wide-angle 50x objective resulting in a spot size of approximately 1µm. The laser power used was 1.7 mW and the exposure time was set to 10 seconds.

For characterization of the impregnated catalysts, Raman spectra from 140 to 1260 cm^{-1} were recorded on the bisected pellet, using a 20x objective. The laser power used is 3.5 mW. Streamline mode [16] was used to generate rapidly high definition 2D chemical images by illuminating with a line of a laser light rather than a spot. Exposure time was defined to 60 seconds and no thermal treatment was carried out. The spatial resolution of each pixel is around 16.2 µm × 16.2 µm. Wire 4.1 software was used for spectra acquisition and to generate Streamline maps. For each streamline analysis, a surface map was defined to prevent from focalization issues and get information about the whole intensities of the spectra when needed. Besides, the intensities used in the different mapping were obtained after a baseline subtraction.

2.3.3. Methodology applied

In this work, MRI-Raman Imaging methodology is applied to characterize the impregnation of γ-alumina first with a complex solution composed of CoMoP and citric acid. Time resolved ^{1}H MRI images were chosen at several points in time during impregnation. The evolution of relaxation times (T_1 and T_2) of water protons in the presence of metallic species (Mo or Co) molybdenum and of the additive (P and CA) allows following their distribution inside the porous medium as contrast agents, as already explained in a previous work [4]. In this study, Raman Imaging analyses were carried out at different times of impregnation to obtain qualitative spatial information about the nature of the molybdenum species throughout the catalyst body and to compare with the MRI images. The system in study is very complex and therefore requires information beyond that obtained at equilibrium in order to better understand the phenomena that take place during impregnation. In this case, we will assume first that the impregnation ends by bisecting the pellet to perform Raman analysis and second that the speciation is not modified.

2.4. Electron Probe Microanalysis measurements

Before Electron Probe Microanalysis (EPMA) measurements, catalysts were calcined at 450°C for 2h. Concerning EPMA sample preparation, catalysts were embedded in a prepolymerized epoxy resin and polished to their diameter. A carbon coating was deposited at the surface of each sample. A semi-quantitative analysis protocol was followed for EPMA measurements. Analyses were performed on a JEOL JXA 8100 electron microprobe at 20 kV and 200 nA. Cobalt, phosphorus and aluminum concentrations were quantified using the Kα lines and molybdenum with Lα line. For P Kα, an overlap correction with the Mo *Ll* line was performed. Under these conditions, detection limits were 380 ppm for Mo, 100 ppm for Co and 4 ppm for P.

The average distribution profile along the cross section was recorded by measuring between three to five different profiles along different 3-fold symmetry axis of the pellets. The analysis step was approximately 50 µm, excluding the cases where the element was in an egg-shell profile. For these ones, an analysis step of 10 µm in each side of the crust was set.

2.5. Image Processing

INDIGO, a proprietary IFPEn software platform was used for data processing. The mean penetration depth of metal ions (and additive) was measured on both MRI images and Streamline Raman maps, whose resolution is numerically increased in the orthogonal plane (x, y) to, respectively, 11 µm x 11 µm and 8 µm x 8 µm by means of high quality spline interpolation [17]. The noise contained in the images is then reduced by a local adaptive filter, a flowing bilateral filter [18], which maintains strong transitions in the image. The area corresponding to the penetration of impregnation solution is obtained by image segmentation with an automatic threshold calculated on the histogram by interclass variance maximization [19]. This procedure has the benefit to be no user dependent. The measure of the mean penetration depth is obtained with the same procedure from [20]. A medial axis is calculated by a morphological watershed from two markers defined as the core and the outside of the catalyst respectively, and propagated on distance function from these two markers. The mean thickness of the penetration, but also the minimum, maximum, and standard deviation, are then obtained from the previous distance function by crossing the points of the medial axis. The different steps of the procedure are illustrated in Fig. 1.

Fig. 1 - Example of processing and analysis of MRI image. From left to right : initial image (resolution 47 µm ×47 µm), increase of resolution by numerical interpolation (resolution 14 µm × 14 µm), automatic segmentation, distance function calculation (red to yellow colors) and medial axis extraction (blue color)

3. Results

3.1. Characterization of CoMoP-CA impregnation solution by Raman spectroscopy

Fig. 2 shows the Raman spectrum obtained for the impregnation solutions in the presence or not of citric acid. In the absence of citrate (see Fig. 2 (a)), the Raman spectrum shows vibration modes $\nu_s(MoO_{2t})$ at 942 and 893 cm^{-1} and the ones $\delta(MoO_{2t})$ at 390 and 369 cm^{-1} indicate the presence of a Strandberg HPA, $H_2P_2Mo_5O_{23}^{4-}$. A similar Raman spectrum is obtained in the presence of citric acid for a CA:Mo ratio of 0.2, see Fig. 2 (b). In this last one, the vibration modes ν_sCOO^- (either 1408 or 1413 cm^{-1}) and νCOOH (1720 cm^{-1}) result from the presence of citrate [21]. For a CA:Mo ratio of 0.7 (see Fig. 2 (c)), the vibration modes $\nu_s(MoO_{2t})$ at 944, 903 and 861 cm^{-1} and $\delta(MoO_{2t})$ at 343, 375 and 383 cm^{-1} are ascribed to a $Mo_4(Cit)_2O_{11}^{4-}$ complex [5,10].

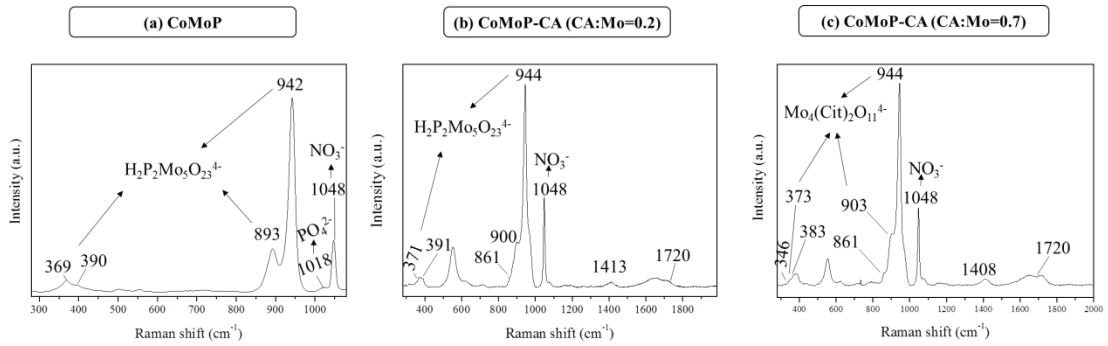

Fig. 2 - Raman spectra for 0.8M [Mo] with (a) Co:Mo=0.3 (molar) and P:Mo=0.4 (molar) and (b) CA:Mo=0.2 (molar) (c) CA:Mo=0.7 (molar) at a pH lower than 1

3.2. Monitoring the impregnation of γ-alumina with CoMoP-CA solution (CA:Mo of 0.2)

Fig. 3 shows the ^{1}H MRI images recorded during the impregnation of γ-alumina with a CoMoP solution with CA:Mo ratio of 0.2. After the initial impregnation, a ring with weak ^{1}H MRI signal is observed near the edges. This crust corresponds to the presence of either P, Mo or CA, but also indicates the absence of Co. Near the core, the intense ^{1}H signal results from the absence of the metallic precursors and additives. A uniform distribution of ^{1}H signal near the core is only obtained after almost 10h of impregnation, which corresponds to the equilibrium state. The low ^{1}H signal near the core indicates an overconcentration of cobalt ions.

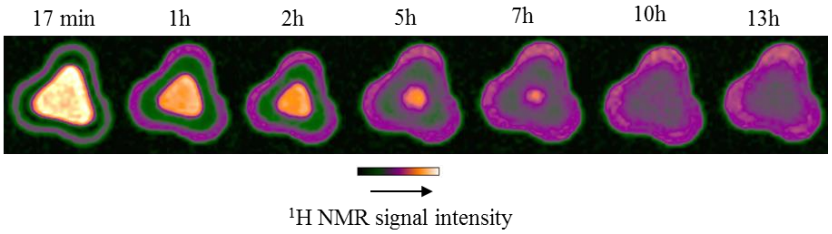

Fig. 3 - Transport of a 0.8 M [Mo] with Co:Mo=0.3 and and P:Mo=0.4 molar and CA:Mo=0.2 molar solution within the porosity of a γ-Al_2O_3 pellet by a spin-echo sequence (FOV=2.5×2.5×8mm; Spatial resolution: 39 × 39 × 125 µm/pixel; Matrix=64×64×8)

The Raman spectra obtained in the bisected pellet at different times of impregnation are gathered in Fig. 4. The analysis of these spectra is done based on Table 3, which gathers the expected vibrations ($\nu(MoO_{2t})$) of the different Mo complexes present in the catalyst pellets.

Table 3 – Characteristic vibrations of all the Mo complexes present in the catalyst pellets [5,7]. The values in gold are the ones used to interpret the Raman spectra.

Species	**$\nu(MoO_{2t})$ (cm^{-1})**	
MoO_4^{2-} in covalent interaction	**920**	
$Mo_7O_{24}^{6-}$	**939**	896
$HMo_7O_{24}^{5-}$	**946**	904

$H_2Mo_7O_{24}^{4-}$	**958**	912			
$P_2Mo_5O_{23}^{6-}$	**956**	926	870		
$HP_2Mo_5O_{23}^{5-}$	**936**	882			
$H_2P_2Mo_5O_{23}^{4-}$	**944**	894			
$H_2PMo_{11}CoO_{40}^{5-}$	1008	**971**	954	886	816
$Mo_4(Cit)_2O_{11}^{4-}$	**944**	901	861		

After almost 5 minutes of impregnation, a Strandberg HPA is deposited in the support, as can be ascribed by vibrations mode $\nu_s(MoO_{2t})$ at 935 cm^{-1}. Moreover, the Raman band at 1049 cm^{-1} results from nitrate ions, which come from cobalt precursor. The band at 1405 cm^{-1} is ascribed to the stretching vibrations of carboxylate group (νCOO^-) [22], which indicates the presence of citrate. After 5h of impregnation, Strandberg HPA is no longer observed in Raman spectra. Heptamolybdates anions in electrostatic interaction with the support are rather observed ($\nu(MoO_{2t})$ 943 cm^{-1}). Additionally, monomeric Mo ions in covalent interaction with γ-alumina are also present ($\nu(MoO_{2t})$ 920 cm^{-1}). At equilibrium, no significant evolution of Mo speciation is observed. In addition, the Raman band characteristic of citrate is no longer observed, which suggests a strong interaction with the support surface.

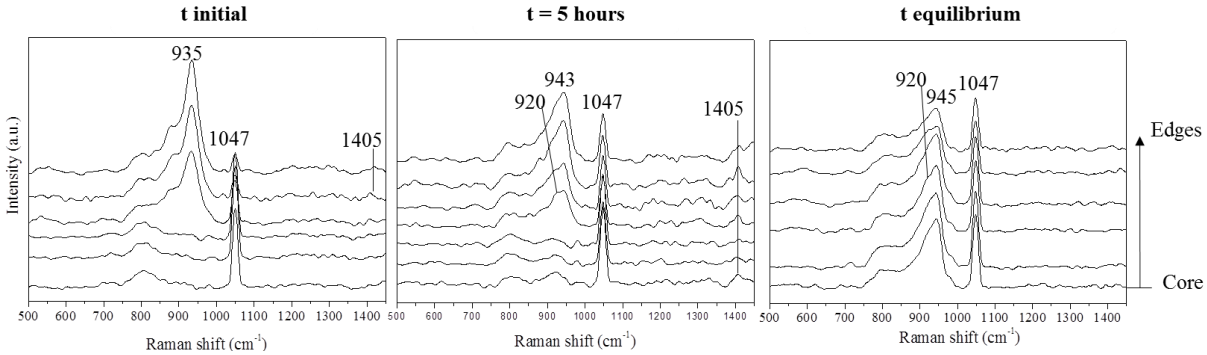

Fig. 4 - Raman spectra (Streamline mode) recorded on γ-alumina impregnated with 0.8 M [Mo] with Co:Mo=0.3, P:Mo=0.4 and CA:Mo=0.2 (molar) at different times of impregnation.

Based on the Raman spectra of Fig. 4, Raman cartographies of the repartition over the pellet of MoO stretching vibrations) were obtained by measuring the maximum of the intensity between 920 and 950 cm^{-1} (see Fig. 5). The thickness (d) corresponding to this region was also measured. The same values of thicknesses are obtained in the corresponding MRI images, regard to the spatial resolution of each technique.

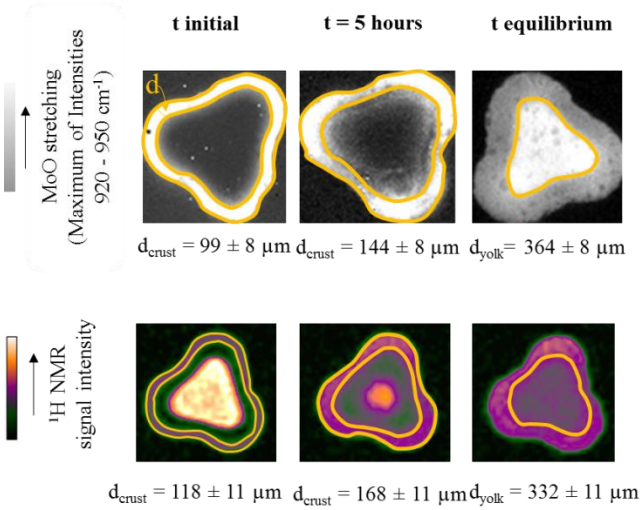

Fig. 5 - Comparison between ^{1}H MRI and Streamline Raman Imaging: images recorded in a γ-alumina support impregnated with 0.8M [Mo] solution with Co:Mo=0.3, P:Mo=0.4 (molar) and CA:Mo=0.2 (molar) at initial time of impregnation (after 17 minutes for MRI images and after 5 minutes for Raman cartography image).

The thicknesses obtained by both techniques are statistically equivalent, which confirms our first hypothesis that the impregnation ends by bisecting the pellet. Besides, in the beginning of impregnation, Mo species are in interaction with phosphorus, which leads to the formation of a Strandberg HPA in an egg-shell distribution (corresponding to a crust thickness of 99 ± 8 µm in Raman image and 118 ± 11 µm in MRI image). As time elapses, Mo ions are either in polymeric or monomeric form and a higher concentration near the edges is still observed (corresponding to a crust thickness of 144 ± 8 µm in Raman image and 168 ± 11 µm in MRI image). Finally, at equilibrium, Mo species are rather in an egg-yolk distribution (corresponding to a yolk thickness of 364 ± 8 µm in Raman image and 332 ± 11 µm in MRI image). Additionally, an overconcentration of Co ions in the same region has already been suggested in the interpretation of MRI images.

3.3. Monitoring the impregnation of γ-alumina with CoMoP-CA solution (CA:Mo of 0.7)

Fig. 6 shows the time-resolved ^{1}H MRI images recorded during impregnation of γ-alumina with a CoMoP-CA solution (CA:Mo ratio of 0.7 molar). The low ^{1}H MRI signal intensity observed near the core suggests the presence of mainly cobalt ions. After two hours of impregnation, this front of low ^{1}H signal achieves the pellet's core, which suggests a faster transport of Co^{2+} ions than in the previous case. Besides that, a crust with a higher ^{1}H MRI signal intensity near the edges is maintained through the impregnation process, which is attributed to the presence of either citrate, phosphorus or a Mo complex. After 7h, no important changes in the distribution profiles are observed, which means that the equilibrium is achieved.

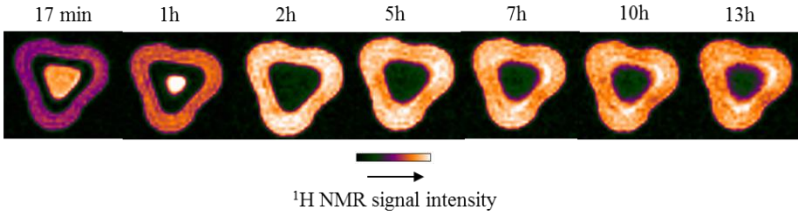

Fig. 6 - Transport of a 0.8 M [Mo] with Co:Mo=0.3 and and P:Mo=0.4 molar and CA:Mo=0.7 molar solution within the porosity of a γ-Al_2O_3 pellet by a spin-echo sequence (FOV=2.5×2.5×8mm; Spatial resolution: 39 × 39 × 125 µm/pixel; Matrix=64×64×8)

Fig. 7 shows the Raman spectra acquired in the bisected catalyst at different times of impregnation. Initially, the vibration modes ν(MoO_{2t}) at 944, 901 and 861 cm^{-1} are characteristic of $Mo_4(Cit)_2O_{11}^{4-}$ complex [5] (see Table 3). Besides, ν(MoO_{2t}) at 956 cm^{-1} is also observed. One can conclude that a mixture of $Mo_4(Cit)_2O_{11}^{4-}$, $H_2Mo_7O_{24}^{4-}$ and/or $H_xP_2Mo_5O_{23}^{(6-x)-}$ is present. Moreover, the presence of citrate is ascribed by ν(COO^-) at 1410 cm^{-1}. After 5h of impregnation, due to the large Raman bands observed, it is not straightforward to identify the different Mo-species. The broad feature between 935 and 950 cm^{-1} can be ascribed to either $H_xP_2Mo_5O_{23}^{(6-x)-}$ or different protonated forms of polymolydbates ($H_xMo_7O_{24}^{(6-x)-}$). Mo-citrate complex is no longer present as indicated by the shift of the main Raman band ($\nu_s(MoO_{2t})$) to higher wavenumber values. The Raman band at 1410 cm^{-1} ($\nu_s(COO)$) is still observed. At equilibrium, the Raman band observed at 971 cm^{-1} indicate the formation of $H_2PMo_{11}CoO_{40}^{5-}$. Once again, a mixture of $H_xP_2Mo_5O_{23}^{(6-x)-}$ and $H_xMo_7O_{24}^{(6-x)-}$ can be ascribed due to the large Raman band between 932 and 965 cm^{-1}.

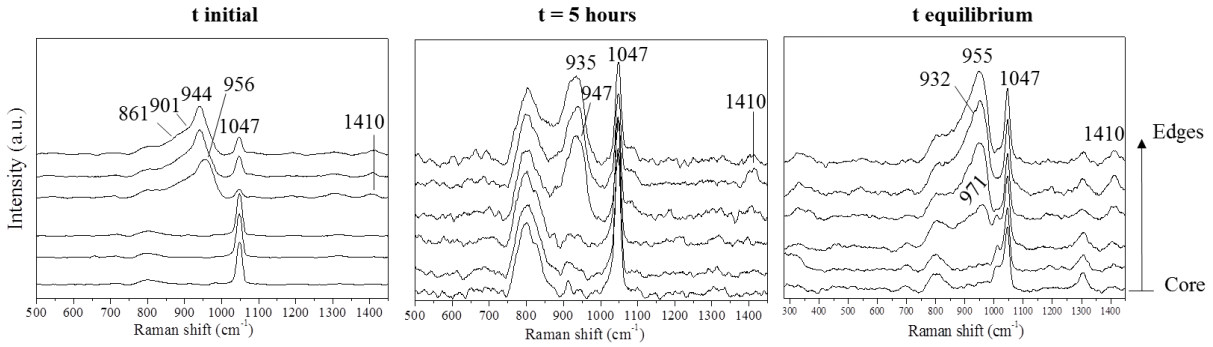

Fig. 7 - Raman spectra (Streamline mode) recorded on γ-alumina impregnated with 0.8 M [Mo] with Co:Mo=0.3, P:Mo=0.4 and CA:Mo=0.7 (molar) at different times impregnation

Raman cartographies were once again obtained concerning the repartition over the pellet of MoO stretching vibrations (maximum of the intensity between 920 and 950 cm^{-1}) (see Fig. 8), which give information concerning spatial distribution of Mo species. The thickness (d) corresponding to this region was also measured. In the corresponding MRI images, almost the same thicknesses are obtained.

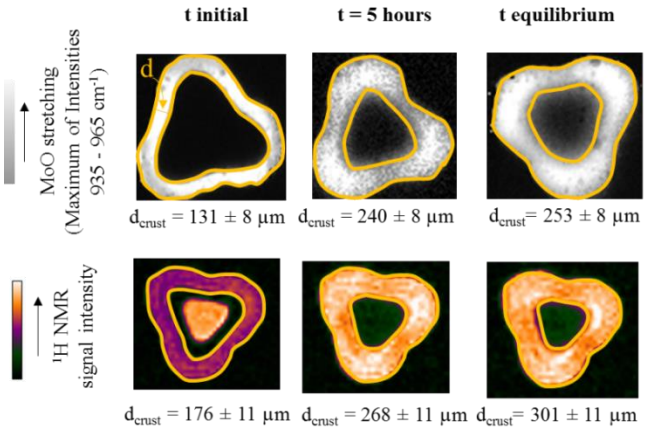

Fig. 8 - Comparison between ^{1}H MRI and Streamline Raman Imaging: images recorded in a γ-alumina support impregnated with 0.8M [Mo] solution with Co:Mo=0.3, P:Mo=0.4 (molar) and CA:Mo=0.7 (molar) at initial time of impregnation (after 17 minutes for MRI images and after 5 minutes for Raman cartography image).

The good agreement obtained between two characterization techniques allows the following interpretations. Right after the initial impregnation, an egg-shell distribution of Mo species either in a Mo-citrate complex or not is observed with a crust thickness of 131 ± 8 µm in Raman image and 176 ± 11 µm in MRI image. As impregnation carries on, hardly Mo-species are present in the core of the support. An egg-shell repartition (corresponding to a crust thickness of 240 ± 8 µm in Raman image and 268 ± 11 µm in MRI image) of Mo species either in a Strandberg HPA or in different protonated forms of polymolydbates are observed. At equilibrium, no important evolution of Mo spatial distribution, even if a heteropolyanion based on Mo, P and Co is observed. Further penetration of Mo ions through support is also indicated by an increase in the crust thickness in both MRI and Raman Images, 301 ± 11 µm and 253 ± 8 µm, respectively. Yet, the difference observed in the thicknesses values is due to an overestimation of the Mo crust in the MRI image, since it is not straightforward to distinguish between Mo and Co ions. Near the core, a local high concentration of Co is suggested, as already mentioned.

Furthermore, at equilibrium, the Raman spectra in Fig. 7 suggest that the Raman band at 971 cm^{-1} is more towards the core, unlike the Raman band at 932 cm^{-1}. To verify this observation, Raman cartographies concerning the intensities of these bands were obtained. Fig. 9 shows that $H_2PMo_{11}CoO_{40}^{5-}$ is indeed found more towards the center of the pellet than $H_xP_2Mo_5O_{23}^{(6-x)-}$ as indicated by the crust thickness of each profile.

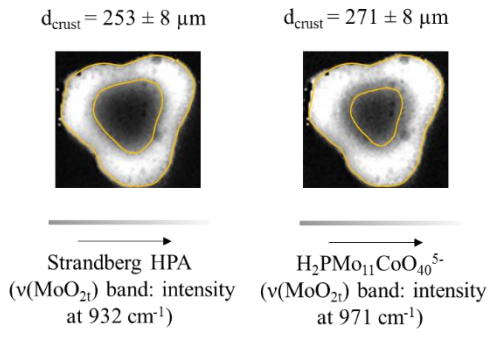

Fig. 9 - Comparison of the crust thickness of the repartition of Raman band at 932cm^{-1} ($H_xP_2Mo_5O_{23}^{(6-x)-}$) and at 971 cm^{-1} (ascribed to $H_2PMo_{11}CoO_{40}^{5-}$)

Finally, the MRI-Raman Imaging results obtained at equilibrium were confronted with EPMA distribution profiles (see Fig. 10). A good agreement among the techniques is obtained taking into account the spatial resolution of each one.

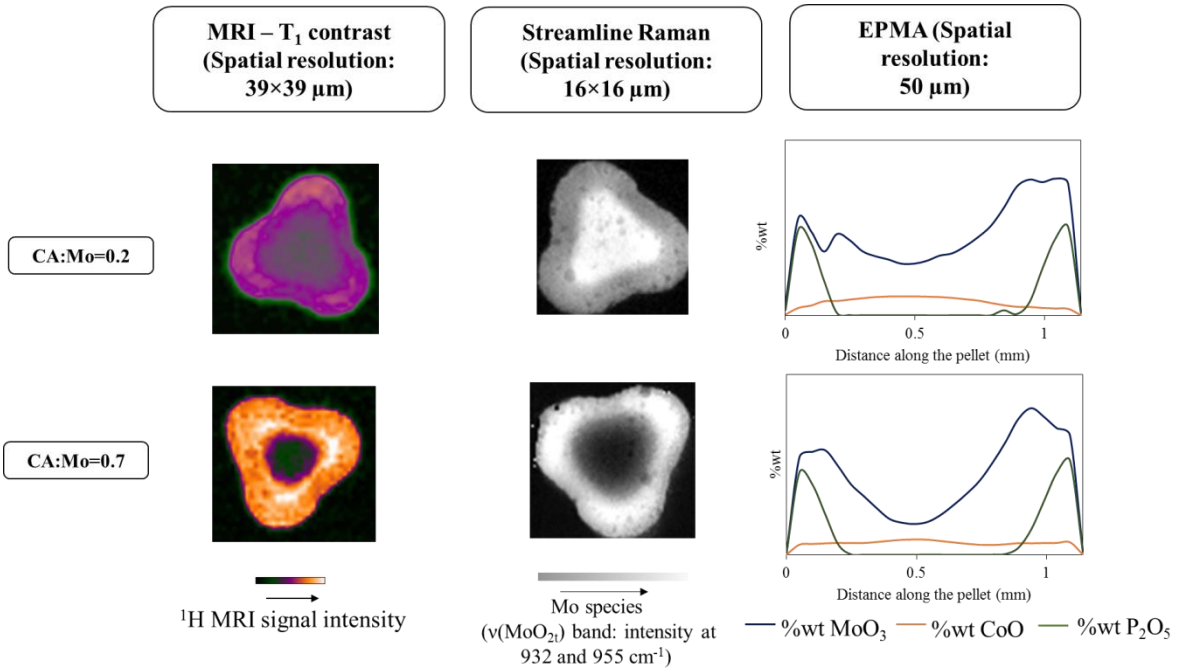

Fig. 10 - Comparison MRI, Raman Imaging and EPMA for CoMoP-AC case: different CA:Mo ratios in impregnation solution were used. Time of 16h is considered as the equilibrium state.

4. Discussion

When impregnation of CoMoP/γ-Al_2O_3 is carried out in the presence of citric acid with CA:Mo molar ratio of 0.2, the presence of a Strandberg HPA ($H_2P_2Mo_5O_{23}^{4-}$) is observed right after the initial impregnation. As impregnation evolves, decomposition of HPA is observed, given rise to polymeric ($Mo_7O_{24}^{6-}$) and monomeric (MoO_4^{2-}) Mo ions.

Indeed, phosphates are known to react with hydroxyl groups of alumina (see Eq. 2), leading to the formation of either linear polyphosphate chains due to the interaction of adjacent phosphorus molecules [23] or an amorphous $AlPO_4$ layer [5,24–26].

$$Al_sOH + HPO_4^{2-} + H^+ \leftrightarrow Al_sHPO_4^- + H_2O \qquad \textbf{Eq. 2}$$

The reaction in Eq. 2 leads to a decrease in free phosphates, which influences the stability of P-type heteropolyanion according to following reaction (see Eq. 3) [5].

$$7P_2Mo_5O_{23}^{6-} + 15H_2O \leftrightarrow 5Mo_7O_{24}^{6-} + 14HPO_4^{2-} + 16H^+ \qquad \textbf{Eq. 3}$$

Due to the decomposition of HPA, $Mo_7O_{24}^{6-}$ ions are formed, which interact electrostatically with the positive surface hydroxyls of alumina (solution pH lower than PZC of γ-alumina). As a result of the buffer effect of

support, these polymeric forms are progressively converted into MoO_4^{2-} due to a pH increase inside the porosity (see Eq. 4).

$$Mo_7O_{24}^{6-} + 8OH^- \leftrightarrow 7MoO_4^{2-} + 4H_2O \quad \textbf{Eq. 4}$$

Unlike $Mo_7O_{24}^{6-}$, MoO_4^{2-} ions interact in a covalent way with the neutral surface hydroxyls, according to Eq. 5 [5,27].

$$2Al_sOH + MoO_4^{2-} \leftrightarrow (Al_s)_2MoO_4 + 2OH^- \quad \textbf{Eq. 5}$$

Apparently, the presence of citrate is not enough to counterweight the increase in pH inside the pores and to maintain a sufficient P:Mo ratio to stabilize the HPA. Moreover, a higher concentration of polymeric Mo ions is found near the edges in relation to monomeric Mo ions in covalent interaction with the support (see Fig. 4). These facts can give information about the local pH. Near the edges, where a higher concentration of both citrate and phosphorus is indicated, a lower local pH is estimated. Towards the core of the support, the concentration of both additives decreases, and a more basic pH promotes the formation of MoO_4^{2-}.

The egg-yolk profile obtained at equilibrium for Mo species highlights a preferential adsorption to phosphates and citrate. In this way, titration of neutral OH groups near the edges occurs and Mo and Co ions can migrate towards the core. This behaviour is the same as already reported in our recent work concerning impregnation of CoMoP/γ-Al_2O_3 in the absence of citric acid [4].

When impregnation solution contains a CA:Mo molar ratio of 0.7, a mixture of Mo-citrate complex and $H_2Mo_7O_{24}^{4-}$ is initially deposited on the support. As impregnation evolves, an evolution of Mo speciation also occurs. At equilibrium, Mo-species are present as either $H_xP_2Mo_5O_{23}^{(6-x)-}$ or different protonated forms of polymolydbates ($H_xMo_7O_{24}^{(6-x)-}$). The formation of an $H_2PMo_{11}CoO_{40}^{5-}$ is also suggested.

The decomposition of Mo-citrate complex present in the initial stages of impregnation highlights two different facts. On one hand, there is a strong affinity of citrate to alumina. On the other hand, a possible competitive adsorption between phosphorus and citrate on alumina surface is observed.

To understand this phenomenon, the surface OH groups of alumina (which is considered equal to 11.8 OH/nm^2 at 573K [28]) and the total amount of citric acid and phosphorus should be evaluated. The density in citric acid molecules in the final catalyst is approximately of 2.3 CA molecules/nm^2, while the density of phosphorus atoms is approximately 0.2 P atoms/nm^2. As already explained, citrate and phosphorus are known to react in the same type of OH surface groups of alumina support. Therefore, the large excess of citrate used has apparently prevented the adsorption of P near the edges of the support. A higher affinity of alumina to citrate rather than to phosphorus is then highlighted. Consequently, the ratio of P:Mo is high enough to prevent the decomposition of Strandberg HPA. Moreover, citrate can also contribute to counterbalance the buffering effect of alumina, which also contributes to the stabilization of Strandberg HPA.

At equilibrium, the formation of $H_2PMo_{11}CoO_{40}^{5-}$ is observed more towards the core. This behaviour had already been observed by Bergwerff et al. [29], which was explained as a result of a concentration gradient of P through the catalyst pellet. Indeed, towards the core of the support, a less quantity of citrate is found, which favours the

adsorption of phosphorus. Consequently, decomposition of Strandberg HPA occurs has P/Mo is not high enough to stabilize the HPA. Hence, decomposition of Strandberg HPA allows the formation of $H_2PMo_{11}CoO_{40}^{5-}$.

Finally, one can observe that for higher concentrations of citrate in the impregnation solution, it takes less time to achieve the equilibrium state. One of the reasons is that the presence of citrate in high contents and its stronger affinity to alumina comparing to the other ions in the impregnation solution contribute to a faster transport of Mo, P and Co through the porosity.

5. General conclusion

In this work, the impact of citric acid on the impregnation of CoMoP/γ-Al_2O_3 catalysts was evaluated thanks to MRI and Raman Imaging. To this end, two different CA:Mo molar ratios in the impregnation solution were tested in order to investigate a possible complexation of Mo by citrate in order to form $Mo_4(Cit)_2O_{11}^{4-}$ complex/

For CA:Mo molar ratio of 0.2 (below the stoichiometric one required, namely 0.5), a higher concentration of Mo-species near the core of the support is observed at the end of the impregnation. Thus, citrate and phosphorus remain at the edges of the catalyst body as a result of strong chemical interactions with the support. Besides, $H_xMo_7O_{24}^{6-}$ or MoO_4^{2-} in electrostatic interaction with the support are also observed. No evidences of a CoMo-citrate complexe are observed. One can consider that the metal promotor ions remain in the form of $Co[H_2O]_6^{2+}$ that can interact with the support. This behaviour is similar when citrate is not present.

On the contrary, for CA:Mo molar ratio of 0.7 (higher than stoichiometric one), the formation of $H_2PMo_{11}CoO_{41}^{5-}$ HPA is observed at the equilibrium state, as a result of a preferential adsorption of alumina to citrate rather than to phosphorus.

Moreover, from the MRI analysis, it was demonstrated that the equilibrium state of impregnation is known to be different depending on the CA:Mo ratio used in the impregnation solution. Therefore, it would be interesting to correlate the difference in equilibrium time with the different impregnation routes for each concentration of citric acid by performing more MRI experiments in the same time.

We demonstrated here that by choosing the adequate CA:Mo molar ratio in the impregnation solution, a close interaction between metal promotor and Mo can be favoured, which might enhance the promoting effect of cobalt. In order to verify this effect, characterization by X-ray photoelectron spectroscopy or even the performance of catalytic tests can be envisaged.

Finally, this work allows a better control of the impregnation step and therefore of the distribution profiles of the metal precursors and in the end of the active phase.

Acknowledgements

The authors thank Prof. Antoine Gédéon and Prof. Flavien Guenneau from CMCP Collège de France (Paris, France) for profitable discussions.

6. References

[1] International Energy Agency, World Energy Outlook 2014, http://www.opec.org/opec_web/en/publications/340.htm (accessed 14.01.2015).

[2] H. Topsøe, B. S. Clausen. F. E. Massoth, Hydrotreating Catalysis Science and Technology, Springer, Berlin, 1996.

[3] H. Jens, Industrial Catalysis: A Practical Approach, 2nd ed., Wiley-VCH, Weinheim, Germany, 2006.

[4] L. Catita, A.-A. Quoineaud, D. Espinat, C. Pichon, O. Delpoux, Application of Magnetic Resonance Imaging and Raman Imaging to study the impact of phosphorus in impregnation of hydrotreatment catalysts, Applied Catalysis A: General 547 (2017) 164–175.

[5] J.A. Bergwerff, T. Visser, Leliveld, Bob R. G., B.D. Rossenaar, de Jong, Krijn P, B.M. Weckhuysen, Envisaging the physicochemical processes during the preparation of supported catalysts: Raman microscopy on the impregnation of Mo onto Al_2O_3 extrudates, J. Am. Chem. Soc. 126 (2004) 14548–14556.

[6] J.A. Bergwerff, van de Water,Leon G.A., A.A. Lysova, I.V. Koptyug, T. Visser, K.P. de Jong, B.M. Weckhuysen, Monitoring the preparation of (Co)Mo/Al_2O_3 extrudates using spatially resolved spectroscopic techniques, Scientific Bases for the Preparation of Heterogeneous Catalysts 162 (2006) 175–186.

[7] Jaap A. Bergwerff, Leon G. A. van de Water, Tom Visser, Peter de Peinder, Bob R. G. Leliveld, Krijn P. de Jong, Bert M. Weckhuysen, Spatially resolved Raman and UV-visible-NIR spectroscopy on the preparation of supported catalyst bodies: controlling the formation of $H_2PMo_{11}CoO_{40}^{5-}$ inside Al_2O_3 pellets during impregnation during impregnation, Chemistry A European Journal 11 (2005) 4591–4601.

[8] J.A. Bergwerff, A.A. Lysova, L. Espinosa-Alonso, I.V. Koptyug, B.M. Weckhuysen, Monitoring transport phenomena of paramagnetic metal-ion complexes inside catalyst bodies with magnetic resonance imaging, Chemistry A European Journal 14 (2008) 2363–2374.

[9] N. Rinaldi, Usman, K. Al-Dalama, T. Kubota, Y. Okamoto, Preparation of Co–Mo/B_2O_3/Al_2O_3 catalysts for hydrodesulfurization: Effect of citric acid addition, Applied Catalysis A: General 360 (2009) 130–136.

[10] O.V. Klimov, A.V. Pashigreva, M.A. Fedotov, D.I. Kochubey, Y.A. Chesalov, G.A. Bukhtiyarova, A.S. Noskov, Co–Mo catalysts for ultra-deep HDS of diesel fuels prepared via synthesis of bimetallic surface compounds, Journal of Molecular Catalysis A: Chemical 322 (2010) 80–89.

[11] C. Radlowski, Method of Making Hydroprocessing Catalyst, US2009/0298677 A1 (2009).

[12] A. J. van Vandillen, R. Terorde, D. J. Lensveld, J. W. Geus, K. P. de Jong, Synthesis of supported catalysts by impregnation and drying using aqueous chelated metal complexes, Journal of Catalysis 216 (2003) 257–264.

[13] H. Y. Carr and E. M. Purcell, Effects of Diffusion on Free Precession in Nuclear Magnetic Resonance Experiments, Physical Review 94 (1954).

[14] S. Meiboom, D. Gill, Modified Spin-Echo Method for Measuring Nuclear Relaxation Times, Rev. Sci. Instrum. 29 (1958) 688.

[15] J. Hennig, A. Nauerth, H. Friedburg, RARE Imaging: A Fast Imaging Method for Clinical MR, Magn. Reson. Med 3 (1986).

[16] Bennet et al., Spectroscopic apparatus with dispersive device for collecting sample data in synchronism with relative movement of a focus, US8179526 B2.

[17] P. Thévenaz, T. Blu, M. Unser, Interpolation revisited, IEE Transactions on Medical Imaging 19 (2000) 739–758.

[18] M. Moreaud, F. Cokelaer, Flowing Bilateral Filter: Definition and Implementations, Image Anal Stereol 34 (2015) 101–110.

[19] N. Otsu, A Threshold Selection Method from Gray-Level Histograms, IEE Transactions on Systems, Man, and Cybernetics SMC-9 (1979) 62–66.

[20] L. Sorbier, A.-S. Gay, A. Fecant, M. Moreaud, N. Brodusch, Measurement of palladium crust thickness on catalysts by optical microscopy and image analysis, Microscopy and microanalysis the official journal of Microscopy Society of America, Microbeam Analysis Society, Microscopical Society of Canada 19 (2013) 293–299.

[21] M. A. Elbagermi, A. I. Alajtal, H. G. M. Edwards, G. H. Azimi, K. D. Verma, I. J. Scowen, Raman spectroscopic and potentiometric studies of acidity level and dissociation of citric acid in aqueous solution, Journal of Applied Chemical Science International (2015) 1–11.

[22] Jacob Arie Bergwerff, Spatially Resolved Spectroscopy on the Preparation of $CoMo/Al_2O_3$ Hydrodesulphurization Catalysts, 2007.

[23] A. Morales, de Agudelo, M. M. Ramírez, F. Hernández, Adsorption mechanism of phosphorus on alumina, Applied Catalysis 41 (1988) 261–271.

[24] Kraus, H., et al., Composition of Impregnation Solutions and Wet Impregnated Mo–P/ -Al2O3 Catalysts as Investigated by 31 P and 95 Mo NMR.

[25] H. Kraus, The Effect of Phosphorus on Oxidic $NiMo(CoMo)/\gamma\text{-}Al_2O_3$ Catalysts: A Solid State NMR Investigation, Journal of Catalysis 170 (1997) 20–28.

[26] W. Cheng, NMR study of the adsorption of phosphomolybdates on alumina, Journal of Catalysis 109 (1988) 163–169.

[27] H. Jeziorowski, H. Knozinger, Raman and Ultraviolet spectroscopic characterization of molybdena on alumina catalysts, The Journal of Physical Chemistry 83 (1979) 1166–1173.

[28] M. Digne, P. Sautet, P. Raybaud, P. Euzen, H. Toulhoat, Hydroxyl Groups on γ-Alumina Surfaces: A DFT Study, Journal of Catalysis 211 (2002) 1–5.

[29] J.A. Bergwerff, van de Water, Leon G A, T. Visser, P. de Peinder, Leliveld, Bob R G, de Jong, Krijn P, B.M. Weckhuysen, Spatially resolved Raman and UV-visible-NIR spectroscopy on the preparation of supported catalyst bodies: controlling the formation of $H_2PMo_{11}CoO_{40}^{5-}$ inside Al_2O_3 pellets during impregnation, Chemistry (Weinheim an der Bergstrasse, Germany) 11 (2005) 4591–4601.